scientific reports

Check for updates

OPEN

Experimental study of the effect of natural fracture curvature on hydraulic fracture propagation behavior

Xun Gong[1,2,3,4,5], Zhijun Jin[1,2]✉, Xinhua Ma[1,3,4,5]✉, Yuyang Liu[3,4,5]✉, Guanfang Li[6] & Yanjun Guo[2,7,8]

The interaction mechanism between hydraulic fractures (HF) and natural fractures (NF) constitutes a critical research focus in hydraulic fracturing optimization. This study systematically investigates the influence of NF curvature on HF propagation behavior through large-scale true triaxial hydraulic fracturing physical simulations. The experiments were conducted on artificial rock specimens containing prefabricated fractures with varying curvature parameters. Results show that the curvature of natural fractures have important effects on the interaction between hydraulic fractures and natural fractures. When the injection rate is constant and the approximation angle is 90°, with the curvature of the natural crack gradually increasing (increasing curvature), the interaction between the hydraulic fracture and the natural fracture shows that the hydraulic fracture passes through the natural fracture and also partially extends along the natural fracture, and gradually changes to the hydraulic fracture extending only along the natural fracture, and then finally exists the natural fracture and extends along the direction of the maximum horizontal principal stress. In addition, the increase in curvature of the natural fractures leads to a decrease in fluid pressure as the hydraulic fractures interact with the natural fractures. The experimental methodology and results contribute to fundamental understanding of fracture propagation mechanics in heterogeneous media, with direct applications to stimulation design in naturally fractured reservoirs.

Keywords Hydraulic fracturing, Natural fracture, Injection rate, Curvature

Unconventional oil and gas reservoirs, characterized by their low porosity and ultra-low permeability, require effective reservoir stimulation techniques to achieve commercial viability in hydrocarbon production[1–3]. Hydraulic fracturing technology is the core technology of reservoir stimulation and plays an important role in the process of oil and gas storage and production. The propagation pattern of hydraulic fractures during fracturing is affected by factors such as the material composition of the rock, diagenesis, geostress, temperature, discontinuity, fracturing fluid, proppant, and well construction parameters, and these factors work together to make it difficult to accurately predict the propagation paths of hydraulic fractures during fracturing, which in turn restricts the volume of reservoir stimulation[4–8]. Among them, the existence of discontinuities such as faults, fractures, and natural fractures is an important reason for the complexity and variability of hydraulic fracture propagation paths. It is found that when hydraulic fractures encounter discontinuities, they may undergo behaviors such as arrested, diverted, penetrated directly, and simultaneously penetrated and diverted[9,10]. The specific behavior that occurs is influenced by factors such as the strength of the natural fracture, production, friction characteristics, geostress, fracturing fluid, and construction parameters[11–16]. The intricate propagation patterns of hydraulic fractures in discontinuous media not only determine the complexity of the resulting fracture network but also

[1]Institute of Energy, Peking University, Beijing 100871, China. [2]School of Earth and Space Sciences, Peking University, Beijing 100871, China. [3]Research Institute of Petroleum Exploration and Development (RIPED), PetroChina, Beijing 100083, China. [4]National Shale Gas Research & Development (Experiment) Center, LangFang 065007, China. [5]Key Laboratory of Coal-rock Gas, CNPC, Langfang 065007, China. [6]Key Laboratory of Shale Gas and Geoengineering, Institute of Geology and Geophysics, Chinese Academy of Sciences, Beijing 100029, China. [7]National Experimental Teaching Demonstrating Center of Earth Sciences(Peking University), Beijing 100871, China. [8]National Virtual Simulation Experimental Teaching Center of Earth Sciences(Peking University), Beijing 100871, China. ✉email: jinzj1957@pku.edu.cn; xinhuam@petrochina.com.cn; yuyang.liu@pku.edu.cn

contribute to the difficulty in accurately modeling hydraulic fracture growth. Understanding these interactions is essential for optimizing hydraulic fracturing designs and improving stimulated reservoir volume (SRV) in unconventional reservoirs.

Rock discontinuities, including joints and natural fractures, are commonly filled with secondary mineralization, exhibiting significantly higher permeability than the surrounding matrix, making them prone to reactivation during hydraulic fracturing[17–20]. The propagation path and morphology of hydraulic fractures (HFs) are critically influenced by natural fractures (NFs), leading to complex interaction behaviors. Scholars conducted a systematic study on the interaction between hydraulic fractures and natural fractures during the fracturing process by using hydraulic fracturing physical experiments and found that during the interaction between hydraulic fractures and natural fractures, the hydraulic fracture may penetrate through the natural fractures directly, be arrested by the natural fractures, or extend along the natural fractures, etc., and the exact occurrence of which depends on the angle of approach (angle of intersection between the hydraulic fracture and natural fractures) and the horizontal principal stress difference[21–23]. The specific situation depends on the approach angle (the angle of intersection between the hydraulic fracture and the natural fracture) and the value of the horizontal principal stress difference[24–27]which establishes the propagation criterion of the hydraulic fracture encountering the natural fracture. Also, scholars conduct hydraulic fracturing tests at the mine site, and the obtained results are more consistent with the laboratory results, and the laboratory conclusions are well validated by using the field construction results[28,29]. Besides external factors, the characteristics of natural fractures themselves, such as orientation, friction characteristics, strength, and size, also affect the results of their interaction with hydraulic fractures[30–32]. As the strength of natural fractures increases, hydraulic fractures tend to penetrate directly through natural fractures. The increase in the size of natural fractures, in turn, is a prerequisite for the generation of a complex network of seams[33–36]. The combined effects of these factors introduce substantial uncertainty in predicting hydraulic fracture propagation paths, resulting in challenges for optimizing fracture network complexity and, consequently, constraining hydrocarbon recovery efficiency in naturally fractured reservoirs.

Although scholars have conducted numerous studies on the interaction between hydraulic fractures and natural fractures, and have achieved certain conclusions and understanding[37–42]. However, according to the field observation, many natural fractures with different degrees of curvature are developed in the rock (Fig. 1), and less research work has been done on the influence of the degree of curvature of natural fractures on the propagation behavior of hydraulic fractures[43,44]. Therefore, this paper firstly prefabricates natural fractures with different degrees of curvature in artificial rock samples, and then conducts true triaxial hydraulic fracturing physical experiments on them and investigates the interaction mechanism between hydraulic fractures and natural fractures with an approach angle of 90°. The results of the study provide some guidance for revealing the interaction mechanism between hydraulic fractures and natural fractures in the fracturing process.

Experimental design and methodology

Experimental setup

The experimental system used in this hydraulic fracturing physical model mainly consists of a true-triaxial hydraulic fracturing experimental machine, a true-triaxial voltage source, an MTS servo pressurization and control device, and a data acquisition and processing system (Fig. 2). As shown in Fig. 3, a cubic rock sample with a side length of 300 mm is placed in the cell of a true-triaxial hydraulic fracturing experimental machine, surrounded by a pressure piston to ensure that controllable pressure can be applied to the six faces of the sample block. The size of the piston is the same as the surface size of the sample, ensuring uniform pressure. The pressure can be controlled by the MTS pump pressure control system, with a maximum pressure output of 30 MPa. Meanwhile, the top of the sample is restrained by a steel plates. The injection power is controlled by an MTS816 servo booster, with a maximum injection pressure of 140 MPa. The highest injection rate that can be delivered is 800 ml/min. Also, an acoustic emission monitoring system is used to locate acoustic emission events during the experimental process, thereby locating the propagation morphology of hydraulic fractures during the fracturing process (Fig. 3).

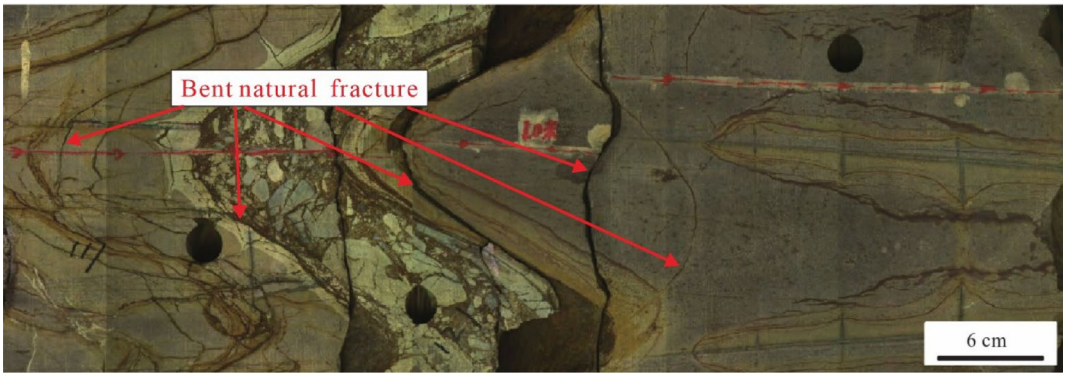

Fig. 1. Natural fractures developed in rocks with curved patterns[44].

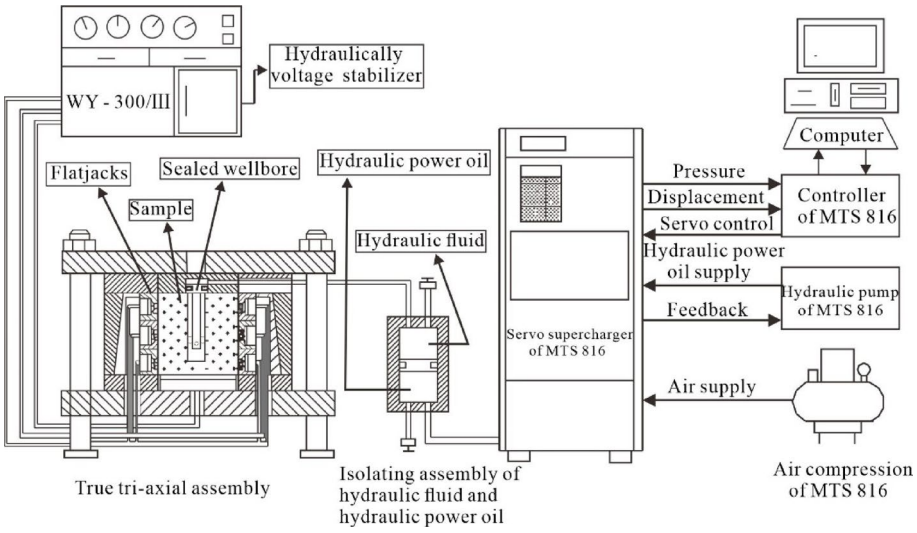

Fig. 2. Schematic of tri-axial experimental equipment[37].

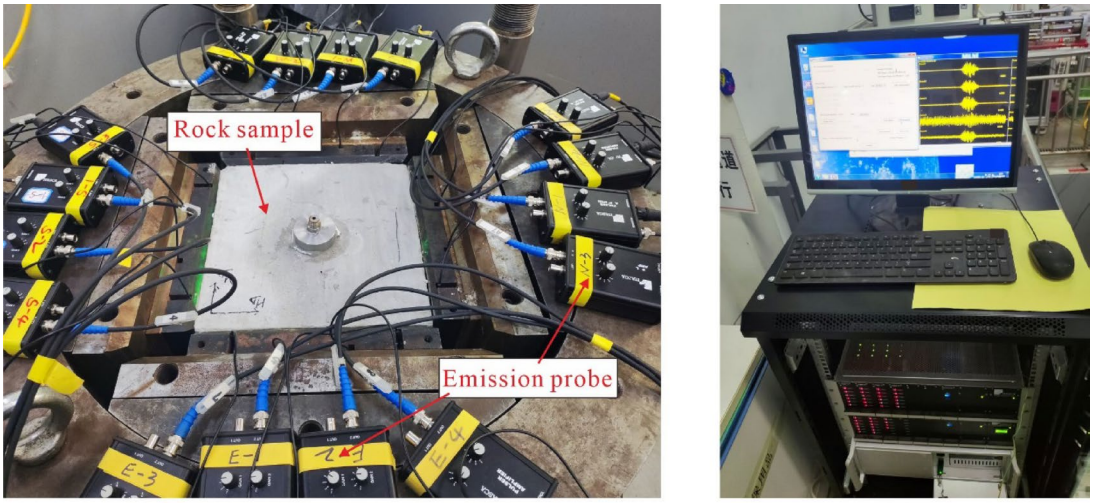

Fig. 3. True triaxial hydraulic fracturing test machine and acoustic emission system. (**a**) Triaxial experimental machine. (**b**) Acoustic emission monitoring device.

An acoustic emission system coupled with a true triaxial hydraulic fracturing system was used to characterize the initiation and propagation patterns of the hydraulic fractures in real time during the hydraulic fracturing process. The acoustic emission system has a total of 16 acoustic sensor probes distributed on the four vertical sides of the cubic rock sample, with four probes on each side, for a total of 16 probes, which are utilized to monitor the damage points in the rock sample during the hydraulic fracturing, and then, based on these acoustic emission data, the determination of the hydraulic fracture geometry is realized (Fig. 3).

Sample preparation

In this experiment, Chinese C80 cement and 40–60 mesh quartz sand were chosen to be mixed in the ratio of 1:1: and then the mixture was made into a cement slurry with water in the ratio of 2:1, and the prepared slurry was placed in a 300 mm cube mould to prepare the rock samples. Moreover, natural fractures were simulated using pieces of paper having a length of 200 mm, a height of 100 mm, and a thickness of 0.8 mm. To ensure that the morphology of the prefabricated natural fractures meets the experimental requirements, a white paper characterized by greater hardness and reduced thickness was deliberately selected. Owing to its superior hardness and enhanced flexibility, this specific paper guarantees the formation of prefabricated fractures that adhere to the experimental specifications during the sample preparation process. Among them, the curvature of the prefabricated natural fractures was defined as the ratio of the difference between the initial length of the prefabricated fracture minus the length of the prefabricated fracture after curving to its initial length (Fig. 4c):

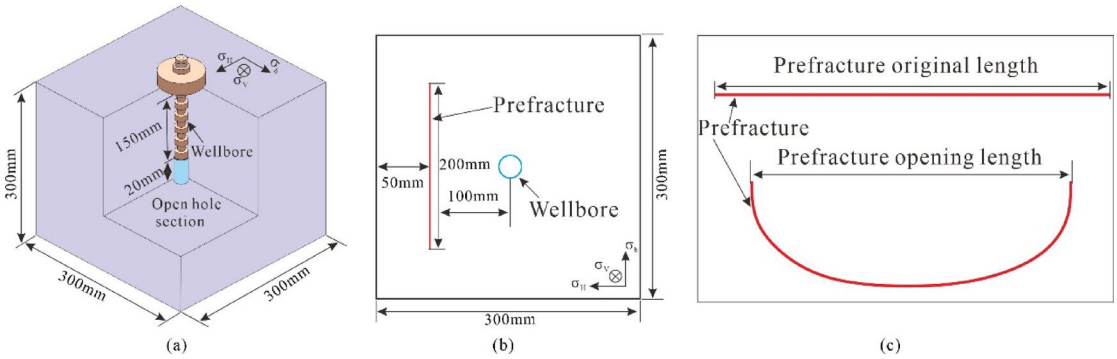

Fig. 4. Schematic diagram of artificial rock sample preparation. (**a**) Design rock sample. (**b**) Top view. (**c**) Prefabricated fracture.

Test	σ_V/MPa	σ_H/MPa	σ_h/MPa	C	Results
gx-1	20	15	10	0	Crossing and Diversion
gx-2	20	15	10	0.25	Crossing and Diversion
gx-3	20	15	10	0.50	Diversion
gx-4	20	15	10	0.75	Diversion

Table 1. Summary of experimental conditions and results obtained.

$$C = \frac{L_i - L_l}{L_i} \tag{1}$$

where C denotes curvature, dimensionless; L_i denotes the initial original length of the prefabricated crack, mm; L_l denotes the length of the prefabricated crack after bending, mm.

In Eq. (1), the larger C is, the greater the degree of bending of the prefabricated crack. By changing the curvature C of the prefabricated natural fracture, the change in the morphology of the prefabricated natural fracture was achieved. In this experiment, the curvature C of prefabricated fracture was set to be 0.75, 0.5, 0.25, and 0. By prefabricating natural fractures with different curvatures, the influence of the morphology of natural fractures on the propagation morphology of hydraulic fractures was thus investigated. The location of the prefabricated cracks is shown in Fig. 4, which is placed 100 mm from the center of the wellbore, the bottom surface is 100 mm from the bottom of the rock sample, the upper surface is 100 mm from the top of the rock sample, and the hydraulic fracture opening direction is unclear from the wellbore (Fig. 4b).

Wellbore design

After the rock sample is prepared, a borehole is drilled into the middle of the sample for processing. The borehole was drilled with a diameter of 25 mm to a depth of 170 mm. Then, the sample was cased by inserting a steel casing with a length of 150 mm, where the open hole section was 20 mm (Fig. 4a,b).

Experimental procedure

The simulation of in-situ stress conditions is the key to hydraulic fracturing experiments. Therefore, this experiment was conducted under normal fault in-situ stress conditions, i.e., vertical stress > maximum horizontal stress > minimum horizontal stress ($\sigma_V > \sigma_H > \sigma_h$). In this case, the vertical stress, maximum horizontal stress, and minimum horizontal stress are 20 MPa, 15 MPa, and 10 MPa, respectively (Table 1).

The fracturing fluid used in the experiment is clean water, and a green fluorescent powder is added to improve the detection ability of hydraulic fractures during the hydraulic fracturing.

During the experiment, the injection rate of fracturing fluid remained constant at 30 ml/min. As the fracturing fluid is injected, the wellbore pressure continues to increase until the wellbore pressure begins to decrease, surface cracks begin to initiate, hydraulic fractures begin to propagate. Injection continues until the fracturing fluid flows out and the sample is broken. After each fluid injection and hydraulic fracturing section of the experiment, the rock blocks are inspected to determine the propagation morphology of hydraulic fractures. After visually inspecting the rock block, use a hammer and chisel to split it open and examine the propagation pattern of internal hydraulic fractures and their interaction with natural fractures.

Finally, photos are taken of each rock block slice and used to these photos to analyze the propagation direction before, during, and after the interaction between hydraulic fractures and prefabricated natural fractures.

Experimental observations and results

In this study, after each hydraulic fracturing experiment on the sample, a hammer and chisel were used to open the rock block along the hydraulic fracture, and the experimental results were observed and recorded. In both two-dimensional planes and three-dimensional spaces, we employ acoustic emission monitoring and tracer techniques to characterize the morphology of generated hydraulic fractures, while simultaneously mapping their spatial three-dimensional configurations. Furthermore, the fracturing process is comprehensively analyzed through integration with the corresponding pumping curves obtained during the fracturing operations.

The fracturing fluid injection rate is 30 ml/min and the angle of approach is 90° (the hydraulic fracture is vertically incident on the natural fracture) when the C is 0, i.e., the gx-1 rock sample exhibits the hydraulic fracture directly crossing the natural fracture simultaneously, some of the fracturing fluids flow along the natural fracture and the natural fracture is reactivated (Fig. 5). As the C increases, more and more fracturing fluid in the gx-2, gx-3 and gx-4 rock samples gradually tend to flow along the natural fractures, the natural fractures are reactivated and the ability of hydraulic fractures to cross the natural fractures directly decreases, and when the C is 0.5, i.e., all of the fracturing fluid flows along the natural fractures in the gx-3 rock samples, resulting in reactivation of the natural fractures while the direct crossing of the natural fracture behavior disappears (Fig. 6).

Furthermore, according to the acoustic emission monitoring results, it was found that during the hydraulic fracturing process, the acoustic emission data points were distributed more uniformly near the near wellbore; after moving away from the wellbore, the acoustic emission data points were relatively reduced; meanwhile, the analysis of the post-pressure fracture morphology found that simple and straight symmetric bi-winged hydraulic fractures were easily generated when the hydraulic fractures were not close to the natural fractures; when the hydraulic fracture interacts with the natural fracture, the morphology of hydraulic fracture becomes curved and complex, and the more complex the morphology of the natural fracture, the more complex is the morphology of the generated fracture network (Figs. 5 and 6) The experimental results are more consistent with the results obtained by Potluri et al.[45] and Dehghan et al.[38] under normal ground stress.

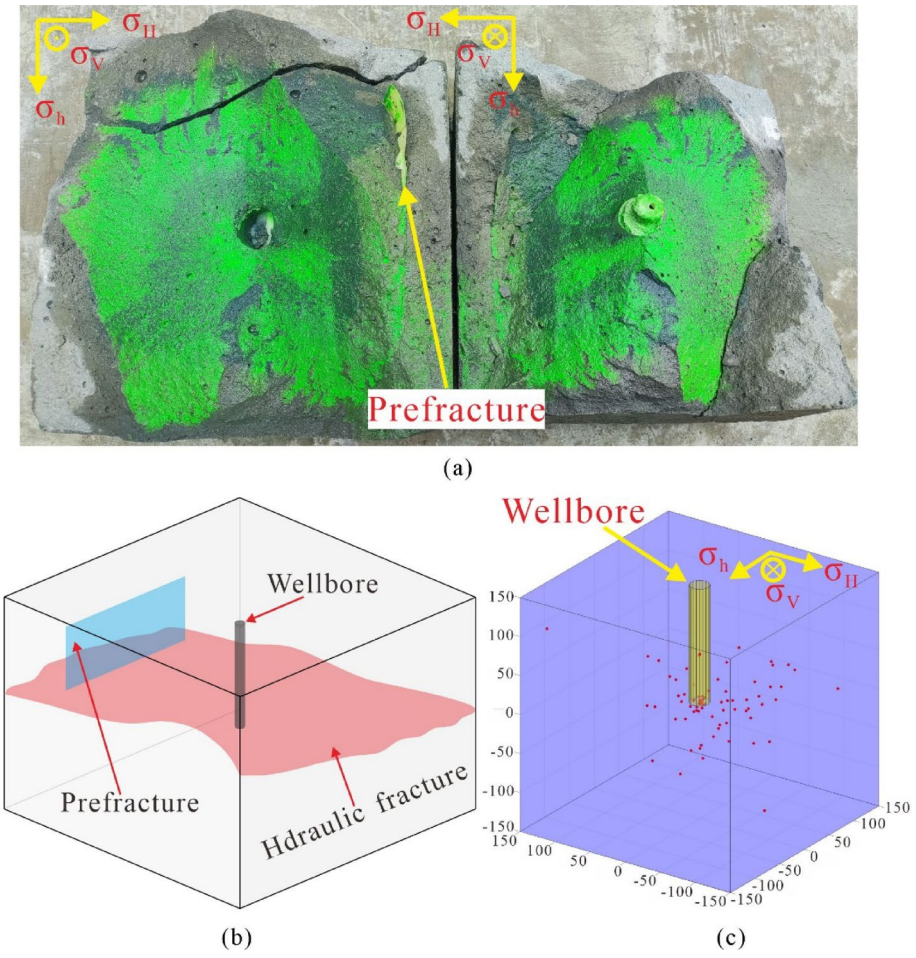

Fig. 5. Hydraulic fracture morphology of rock samples with a curvature of 0.(**a**) Geometry of hydraulic fractures. (**b**) Three-dimensional morphology of fractures. (**c**) Acoustic emission monitoring results.

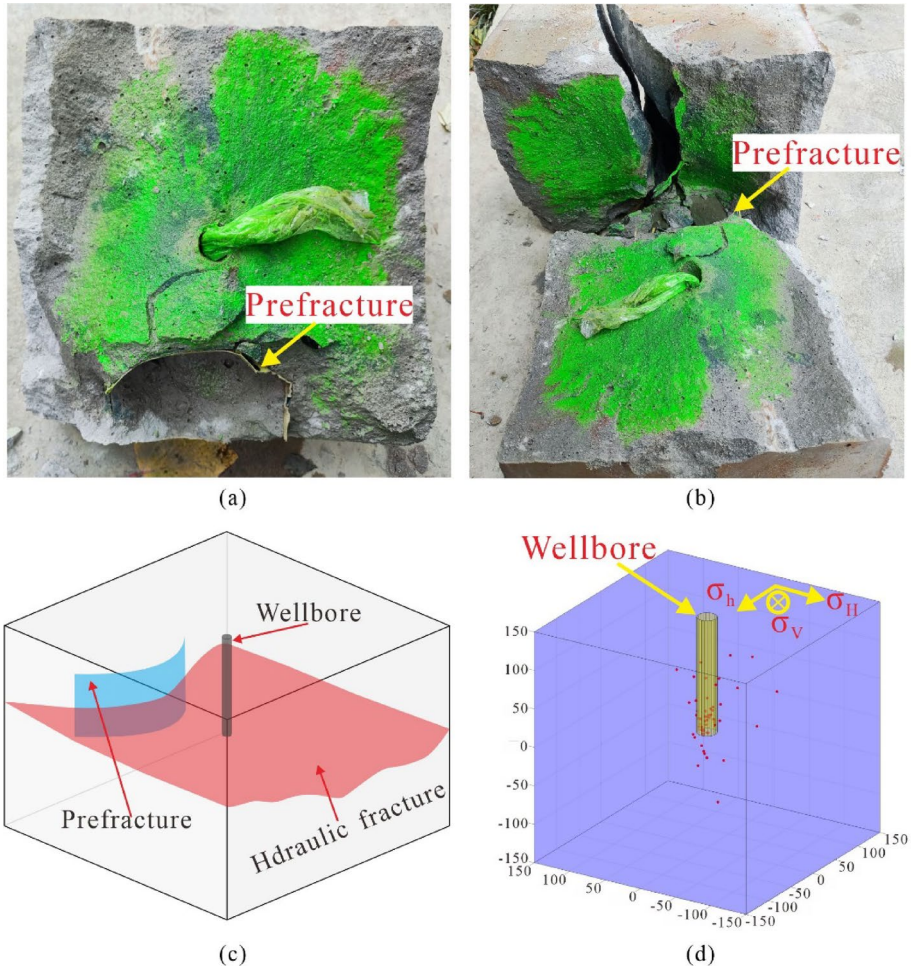

Fig. 6. Hydraulic fracture morphology of rock samples with a curvature of 0.5. (**a**) and (**b**) Geometry of hydraulic fractures. (**c**) Three-dimensional morphology of fractures. (**d**) Acoustic emission monitoring results.

Discussion

Analysis of the behaviour of hydraulic fractures interacting with natural fractures

Many scholars have conducted extensive research on the interaction mechanism between hydraulic fractures and natural fractures and proposed the interaction criteria, and Blanton[21,22]Warpinski and Teufel[23] concluded from laboratory hydraulic fracturing physical modeling experiments and hydraulic fracturing mine experiments, respectively, that when a hydraulic fracture encounters a natural fracture, the hydraulic fracture can cross the natural fracture, be arrested by the natural fracture and extend along the natural fracture, depending on the angle of approach and the magnitude of horizontal principal stress difference. The hydraulic fracture may cross the natural fracture, the hydraulic fracture is arrested by the natural fracture, and the hydraulic fracture extends along the natural fracture, depending on the angle of approach and the magnitude of the horizontal principal stress difference. However, this criterion mainly focuses on the initial interaction behavior when the hydraulic fracture encounters the natural fracture and does not take into account the later interaction behavior. Potluri et al.[45] evaluated the extension of the hydraulic fracture after its interaction with the natural fracture using the method of Warpinski and Teufel's[23]. Three main possible patterns were introduced, i.e., traversal and propagation starting from the tip of the natural fracture, as well as propagation and breakthrough at the weak points of the natural fracture surface.

Zhou and Dehghan et al.[37,38] also observed three types of interactions between hydraulic fractures and natural fractures on an experimental basis, which is the same as that observed by Warpinski and Teufel's[23]. Moreover, Dehghan et al.[38] investigated the effect of the inclination and orientation of natural fractures on the propagation of hydraulic fractures and concluded that hydraulic fractures either propagate along the direction of the maximum horizontal geostress or in the direction of the height of natural fractures under normal fault regime geostress conditions. Based on this, this paper analyses the influence of the morphology change of the natural fractures on the hydraulic fracture propagation behavior when the hydraulic fracture acts vertically on the natural fracture, and finds that the hydraulic fracture is more likely to generate simple, straight, and symmetric biplane hydraulic fractures when it does not encounter the natural fracture; when the hydraulic fracture interacts with the natural fracture, the morphology of hydraulic fracture becomes curved and complex, and the more complex the morphology of the natural fracture, the more complex the generated fracture network

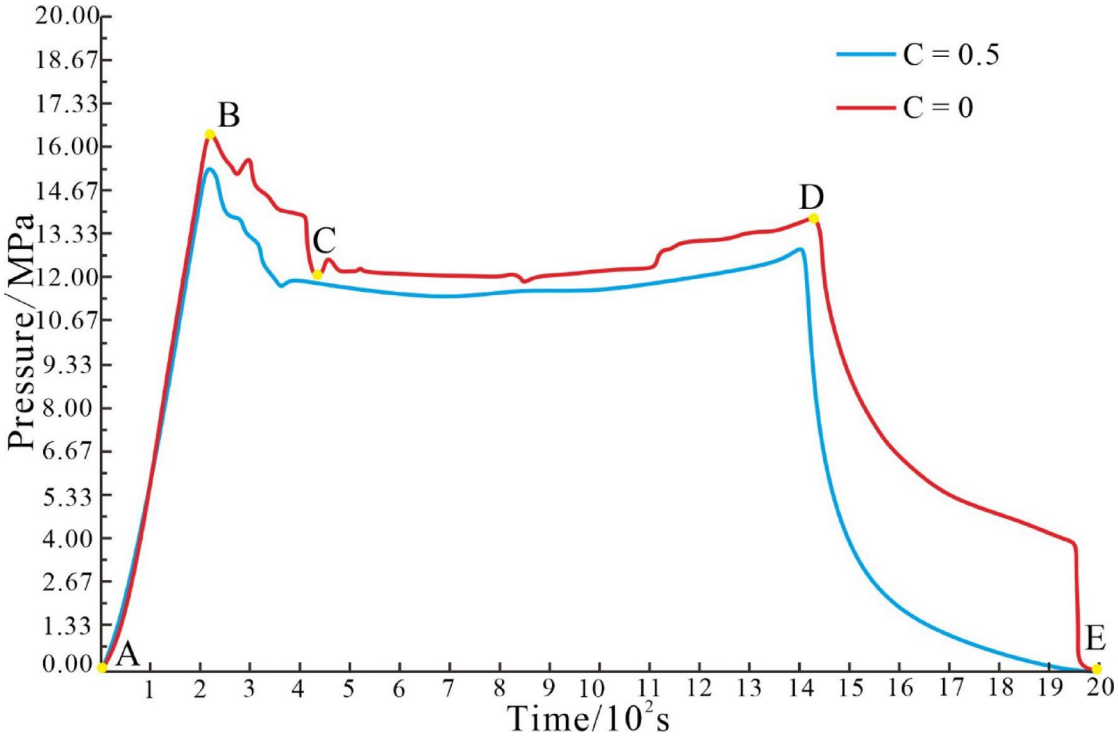

Fig. 7. Fluid pressure pumping curve.

morphology is. The more complex the natural fracture morphology, the more complex the generated fracture network morphology (Figs. 5 and 6). Meanwhile, the distribution of acoustic emission data points provides a good validation of the near-wellbore fracture morphology. The findings of Potluri et al.[45] and Dehghan et al.[38] were confirmed by the study.

In addition, when the injection rate is constant and the curvature is small, hydraulic fracture and natural fracture interactions mainly show hydraulic fracture crossing the natural fracture and extending partially along the natural fracture. As the degree of curvature of the natural fractures increases (i.e., the C increases), more fracturing fluid is diverted by the natural fractures, the natural fractures are reactivated, and the phenomenon of the hydraulic fractures crossing directly through the natural fractures diminishes. Further, when the curvature of the natural fracture is 0.5, the perpendicular interaction between the hydraulic fracture and the natural fracture exhibits that the hydraulic fracture extends along the natural fracture and then along the direction of the maximum horizontal principal stress, and the phenomenon of the hydraulic fracture crossing the natural fracture disappears. Therefore, under the normal state of geostress, the injection rate of fracturing fluid is constant, and the approach angle between hydraulic fracture and natural fracture is 90°, when the C is less than 0.5, when the hydraulic fracture extends to the natural fracture, it mainly occurs that the hydraulic fracture crosses the natural fracture directly and the hydraulic fracture crosses the natural fracture while the natural fracture is partially activated (Fig. 5); when the C is greater than or equal to 0.5, the hydraulic fracture and natural fracture interaction presents a hydraulic fracture turning along the natural fracture (Fig. 6). It can be inferred that when the injection rate is large and the approach angle between the hydraulic fracture and the natural fracture is 90°, the hydraulic fracture will directly cross the natural fracture when the hydraulic fracture extends to the natural fracture; keeping the angle of approach constant, with the gradual decrease of the injection rate, the hydraulic fracture gradually transforms from directly crossing the natural fracture to the hydraulic fracture crossing the natural fracture and simultaneously extending along the natural fracture. When the injection rate is constant and the approach angle is 90°, the hydraulic fracture gradually changes from extending along the natural fracture while crossing the natural fracture to extending only along the natural fracture as the natural fracture morphology becomes more and more curved (C increases) and finally extends along the direction of the maximum horizontal principal stress. Therefore, when hydraulic fractures act on natural fractures, the fluid injection rate and natural fracture morphology play an important role in controlling the interaction between hydraulic fractures and natural fractures, which in turn affects the complexity of the generated fracture network.

Analysis of fluid pressure changes

Subsequent analysis of the fracturing process pumping curves revealed consistent patterns across experiments (Fig. 7). Therefore, we focused on the case with curvature 0, which demonstrated four distinct stages: AB, BC, CD, and DE. The AB stage represents a phase of rapid fluid pressure increase. Upon reaching point B, the pressure attains its maximum value (rock fracture pressure), initiating fracture formation in the rock sample. This is followed by the BC stage, where the accumulated energy dissipates as the hydraulic fracture propagates, reaching its minimum at point C. The CD stage commences with fluid injection, causing pressure to rise again.

This pressure increase is attributed to the interaction between hydraulic fractures and prefabricated fractures. The pressure continues to climb until reaching point D, where it attains a secondary peak. At this juncture, the pressure pump is deactivated, and fluid injection ceases. Subsequently, during the DE stage, the fluid pressure gradually decreases as fracture expansion continues until complete pressure dissipation. The observed variations in rock fracture pressure are primarily attributed to sample preparation and drying processes. Notably, the pressure difference between curvatures 0 and 0.5 during the CD stage can be explained by two factors: (1) sample variability, and (2) energy accumulation dynamics. Specifically, the curvature 0 configuration requires greater energy accumulation for vertical penetration through prefabricated fractures, whereas the curvature 0.5 configuration facilitates fluid flow through curved natural fractures, resulting in reduced energy accumulation and consequently lower fluid pressure.

Conclusion

(1) When hydraulic fractures act on natural fractures, the injection rate of fracturing fluid and the morphology of natural fractures during hydraulic fracturing play an important role in controlling the interaction behavior of hydraulic fractures with natural fractures. When the hydraulic fracture does not encounter the natural fracture, it is easier to generate simple, straight, and symmetric bi-wing hydraulic fracture; when the hydraulic fracture interacts with the natural fracture, the hydraulic fracture morphology becomes curved and complex, and the more complex the natural fracture morphology is, the more complex the morphology of the generated fracture network is.
(2) Other conditions remain unchanged, when the hydraulic fracture acts on the natural crack, with the increase of the degree of curvature of the natural crack (curvature increase), the hydraulic fracture gradually changes from crossing the natural fracture and expanding along the natural fracture to extending only along the natural fracture, and penetrating the NF and extending along the direction of the maximum horizontal principal stress.
(3) Other conditions remain unchanged, when the hydraulic fracture acts perpendicularly on the natural fracture, with the decrease in the injection rate of fracturing fluid, the hydraulic fracture gradually changes from directly crossing the natural fracture to crossing the natural fracture and turning along the natural fracture simultaneously.
(4) The curvature of natural fractures significantly influences energy accumulation and fluid pressure during hydraulic fracturing. Specifically, increased natural fracture curvature results in reduced energy accumulation when hydraulic fractures intersect with natural fractures. This phenomenon directly affects fluid pressure dynamics: higher natural fracture curvatures correspond to lower fluid pressures during hydraulic-natural fracture interactions.

Data availability

All data that support the findings of this study are available from the corresponding author upon reasonable request.

Received: 18 January 2025; Accepted: 12 June 2025
Published online: 01 July 2025

References

1. Jarvie, D. et al. Unconventional shale-gas systems: the Mississippian barnett shale of north-central Texas as one model for thermogenic shale-gas assessment. *Aapg Bull.* **91** (4), 475–499 (2007).
2. Ross, D. & Bustin, R. The importance of shale composition and pore structure upon gas storage potential of shale gas reservoirs. *Mar. Petrol. Geol.* **26** (6), 916–927 (2009).
3. Zou, C. et al. Geological characteristics and resource potential of shale gas in China. *Petrol. Explor. Dev.* (6), 641–653 (2010).
4. Zhao, Z. et al. A laboratory investigation of fracture propagation induced by supercritical carbon dioxide fracturing in continental shale with interbeds. *Eng. Geol.* **166**, 739–746 (2018).
5. Li, Z., Li, L. & Huang, B. Numerical investigation on the propagation behavior of hydraulic fractures in shale reservoir based on the DIP technique. *J. Pet. Sci. Eng.* **154**, 302–314 (2017).
6. Wang, L. et al. June. The effect of natural fracture complexity on fracture propagation in deep shale based on true tri-Axial experiments. *Paper presented at the 53rd U.S. Rock Mechanics/Geomechanics Symposium* (2019).
7. Kamali, A., Ghassemi, A. & Kumar, D. 3D modeling of hydraulic and natural fracture interaction. *Rock. Mech. Rock. Eng.* **56** (2), 875–893 (2023).
8. Zhou, Q. et al. Fracture toughness anisotropy in shale under deep in situ stress conditions. *Rock. Mech. Rock. Eng.* **56**, 7535–7555 (2023).
9. Zhang, Y. et al. Numerical study of hydraulic fracture propagation in inherently laminated rocks accounting for bedding plane properties. *J. Pet. Sci. Eng.* **210**, 109798 (2022).
10. Guo, T. et al. Physical simulation of hydraulic fracturing of large-sized tight sandstone outcrops. *Spe J.* **26** (01), 372–393 (2021).
11. Zou, J. et al. Complex hydraulic-fracture-network propagation in a naturally fractured reservoir. *Comput. Geotech.* **135**, 104165 (2021).
12. Zhang, J. et al. Experiments and analysis on the influence of multiple closed cemented natural fractures on hydraulic fracture propagation in a tight sandstone reservoir. *Eng. Geol.* **281**, 105981 (2021).
13. Hu, L. & Ghassemi, A. Laboratory-scale investigation of the slippage of a natural fracture resulting from an approaching hydraulic fracture. *Rock. Mech. Rock. Eng.* **54**, 2547–2558 (2021).
14. Lei, Q., Doonechaly, N. & Tsang, C. Modelling fluid injection-induced fracture activation, damage growth, seismicity occurrence and connectivity change in naturally fractured rocks. *Int. Int. J. Rock. Mech. Min.* **138**, 104598 (2021).
15. Zhang, B. et al. Numerical simulation of fracture propagation and production performance in a fractured geothermal reservoir using a 2D FEM-based THMD coupling model. *Energy* **273**, 127175 (2023).
16. Xie, Z. et al. Influence of natural fractures on the propagation of hydraulic fractures in hot dry rock. *Nat. Gas Ind. B.* **42** (4), 63–72 (2022).

17. Kresse, O. et al. Numerical modeling of hydraulic fractures interaction in complex naturally fractured formations. *Rock. Mech. Rock. Eng.* **46** (3), 555–568 (2013).
18. Tan, P. et al. Analysis of hydraulic fracture initiation and vertical propagation behavior in laminated shale formation. *Fuel* **206**, 482–493 (2017).
19. Cheng, W., Jin, Y. & Chen, M. Reactivation mechanism of natural fractures by hydraulic fracturing in naturally fractured shale reservoirs. *J. Nat. Gas Sci. Eng.* **23**, 431–439 (2015).
20. Bakhshi, E. et al. Lattice numerical simulations of lab-scale hydraulic fracture and natural interface interaction. *Rock. Mech. Rock. Eng.* **52** (5), 1315–1337 (2019).
21. Blanton, T. An experimental study of interaction between hydraulically induced and pre-existing fractures. *SPE Unconventional Resources Conference/Gas Technology Symposium*. SPE-10847-MS. (1982).
22. Blanton, T. Propagation of hydraulically and dynamically induced fractures in naturally fractured reservoirs. *SPE Unconventional Gas Technology Symposium. Society of Petroleum Engineers* (1986).
23. Warpinski, N. & Teufel, L. Influence of geologic discontinuities on hydraulic fracture propagation (includes associated papers 17011 and 17074). *J. Pet. Technol.* **139** (02), 209–220 (1987).
24. Renshaw, C. & Pollard, D. An experimentally verified criterion for propagation across unbounded frictional interfaces in brittle, linear elastic materials. *Int. J. Rock. Mech. Min. Sci. Geomech. Abstracts*. **32** (3), 237–249 (1995).
25. Gu, H. & Weng, X. Criterion for fractures crossing frictional interfaces at non-orthogonal angles. *44th US rock mechanics symposium and 5th US-Canada rock mechanics symposium* OnePetro (2010).
26. Gu, H. et al. Hydraulic fracture crossing natural fracture at nonorthogonal angles: a criterion and its validation. *Spe Prod. Oper.* **27**(01), (2012). 20 – 6 (.
27. Fisher, K. & Warpinski, N. Hydraulic-Fracture-Height growth: real data. *Spe Prod. Oper.* **27** (01), 8–19 (2012).
28. Brinkley, K. et al. January. Redefining Recoverable Reserves in the Eagle Ford: Refracs and Infill Development Lessons Learned From the Hydraulic Fracturing Test Site 1 (HFTS) Phase 3. *Paper presented at the SPE Hydraulic Fracturing Technology Conference and Exhibition*, The Woodlands, Texas, USA, (2023).
29. Fu, W. et al. Developing upscaling approach for swarming hydraulic fractures observed at hydraulic fracturing test site through multiscale simulations. *Spe J.* **26** (05), 2670–2684 (2021).
30. Li, J. et al. Hydraulic fracture propagation with complex natural fracture network in Lacustrine shale oil reservoirs. *SPE Annual Caspian Technical Conference*. SPE D031S015R003. (2023).
31. Li, J. & Wu, K. An efficient model for hydraulic fracture height growth considering the effect of bedding layers in unconventional shale formations. *Spe J.* **27** (06), 3740–3756 (2022).
32. Wang, S. et al. Modeling interactions between hydraulic and closed natural fractures in brittle crystalline rocks: A Fluid–Solid coupling Grain-Based approach for characterizing microcracking behaviors. *Rock. Mech. Rock. Eng.* **57** (2), 889–920 (2024).
33. Guo, Y., Huang, L. & Li, X. Experimental and numerical investigation on the fracture behavior of deep anisotropic shale reservoir under in-situ temperature. *Energy* **282**, 128969 (2023).
34. Zeng, Q. et al. Numerical investigation of hydraulic fracture propagation interacting with bedding planes. *Eng. Fract. Mech.* **291**, 109575 (2023).
35. Pidho, J. et al. Analysis of interaction of hydraulic fractures with natural fractures and bedding planes in layered formation through cohesive zone modelling. *Theor. Appl. Fract. Mec.* **123**, 103708 (2023).
36. Li, Y. et al. Influence of preexisting discontinuities on hydraulic fracture complexity in a naturally fractured reservoir. *Eng. Geol.* **311**, 106919 (2022).
37. Zhou, J. et al. Analysis of fracture propagation behavior and fracture geometry using a tri-axial fracturing system in naturally fractured reservoirs. *Int. Int. J. Rock. Mech. Min.* **45** (7), 1143–1152 (2008).
38. Dehghan, A. et al. The effect of natural fracture dip and strike on hydraulic fracture propagation. *Int. J. Rock. Mech. Min.* **75**, 210–215 (2015).
39. Xiong, D. & Ma, X. Influence of natural fractures on hydraulic fracture propagation behaviour. *Eng. Fract. Mech.* **276**, 108932 (2022).
40. Li, J. et al. Study on the influence of natural fracture modeling on hydraulic fracture propagation for horizontal Wells in unconventional resource-A case study from China. *Abu Dhabi International Petroleum Exhibition and Conference SPE*. D032S180R007. (2022).
41. Olson, J., Bahorich, B. & Holder, J. Examining hydraulic fracture-natural fracture interaction in hydrostone block experiments. *SPE Hydraulic Fracturing Technology Conference and Exhibition*. SPE-152618-MS. (2012).
42. Rahman, M., Aghighi, A. & Rahman, S. Interaction between induced hydraulic fracture and pre-existing natural fracture in a poro-elastic environment: Effect of pore pressure change and the orientation of natural fracture. *SPE Asia Pacific Oil and Gas Conference and Exhibition*. SPE-122574-MS. (2009).
43. Du, X. Y. et al. Characteristics and controlling factors of natural fractures in deep lacustrine shale oil reservoirs of the Permian Fengcheng Formation in the Mahu Sag, Junggar Basin, *China. J Struct Geol* **175** 104923 (2023).
44. Zeng, L. B. et al. Natural fractures in deep to ultra-deep tight reservoirs: distribution and development. *Shiyou Yu Tianranqi Dizhi.* **45** (1), 1–14 (2024).
45. Potluri, N., Zhu, D. & Hill, A. Effect of natural fractures on hydraulic fracture propagation. *SPE European Formation Damage Conference and Exhibition*. SPE-94568-MS. (2005).

Acknowledgements

The work was supported by the funding of the Project of R&D Department of Petrochina (No. 2024DJ8705).

Author contributions

Xun Gong: Conceptualization, methodology, visualization, software, writing—original draft, review & editing, and validation. Zhijun Jin: Conceptualization, methodology, and review & editing. Xinhua Ma: Conceptualization, methodology, funding acquisition, and review & editing. Yuyang Liu: funding acquisition, and review & editing. Guanfang Li: review & editing. Yanjun Guo: Acoustic emission data processing and analysis.

Funding

This research was funded by the project of R&D Department of Petrochina (No. 2024DJ8705).

Declarations

Competing interests

The authors declare no competing interests.

Consent to publish
This article was submitted and published with the consent of all authors.

Additional information
Correspondence and requests for materials should be addressed to Z.J., X.M. or Y.L.

Reprints and permissions information is available at www.nature.com/reprints.

Publisher's note Springer Nature remains neutral with regard to jurisdictional claims in published maps and institutional affiliations.